Soft Matter

Understanding the effect of liquid crystal content on the phase behavior and mechanical properties of liquid crystal elastomers

Journal:	*Soft Matter*
Manuscript ID	SM-ART-04-2022-000480.R1
Article Type:	Paper
Date Submitted by the Author:	03-Jun-2022
Complete List of Authors:	Barnes, Morgan; Cambridge University, Engineering; Rice University, Materials Science and NanoEngineering Cetinkaya, Sueda; Rice University, Chemical and Biomolecular Engineering Ajnsztajn, Alec; Rice University, Materials Science and NanoEngineering Verduzco, Rafael; Rice University, Chemical and Biomolecular Engineering

Soft Matter

ARTICLE TYPE

Cite this: DOI: 10.1039/xxxxxxxxxx

Understanding the effect of liquid crystal content on the phase behavior and mechanical properties of liquid crystal elastomers

Morgan Barnes[a], Sueda Cetinkaya[b], Alec Ajnsztajn[a], and Rafael Verduzco[ab]

Received Date
Accepted Date

DOI: 10.1039/xxxxxxxxxx

www.rsc.org/journalname

Liquid crystal elastomers are stimuli-responsive, shape-shifting materials. They typically require high temperatures for actuation which prohibits their use in many applications, such as biomedical devices. In this work, we demonstrate a simple and general approach to tune the order-to-disorder transition temperature (T_{ODT}) or nematic-to-isotropic transition temperature (T_{NI}) of LCEs through variation of the overall liquid crystal mass content. We demonstrate reduction of the T_{NI} in nematic LCEs through the incorporation of non-mesogenic linkers or the addition of lithium salts, and show that the T_{NI} varies linearly with liquid crystal mass content over a broad range, approximately 50 degrees C. We also analyze data from prior reports that include three different mesogens, different network linking chemistries, and different alignment strategies, and show that the linear trend in T_{ODT} with liquid crystal mass content also holds for these systems. Finally, we demonstrate a simple approach to quantifying the maximum actuation strain through measurement of the soft elastic plateau and demonstrate applications of nematic LCEs with low T_{ODT}s, including the first body-responsive LCE that curls around a human finger due to body heat, and a fluidic channel that directionally pumps liquid when heated.

1 Introduction

Liquid crystal elastomers (LCEs) mimic human muscle as they are soft materials that undergo macroscopic (>100% strain) reversible shape changes when exposed to stimuli such as heat, light, and electric fields.[1–3] As such, LCEs have many potential applications including in biomedical devices, soft robotics, and sensors.[4–6] The most robust and well-developed methods for LCE actuation utilize heating, either photothermal or resistive, to induce shape changes[7–11] However, many LCEs have prohibitively high nematic-to-isotropic transition temperatures (T_{NI} > 100 °C) and cannot be easily actuated under ambient conditions or near body temperature.[12–15] Therefore, there is a need for reducing the LCE nematic-to-isotropic transition temperature while maintaining the ability to program complex shape changes or adding additional functionality. This would expand the practical application of LCEs, including for implantable LCE devices tha respond to mild heating and as photo-responsive soft-robotics that do not require high light intensities.

In recent work, the actuation temperature of LCEs has been lowered by incorporating different liquid crystal mesogens, chemical linkers, and crosslinkers into the network.[16–19] For example, Saed et al. showed that increasing the length of the molecular linker between liquid crystalline mesogens significantly lowered the T_{NI} and that T_{NI} increased with crosslink density.[20–22] Similarly, Zhang et al. demonstrated that the inorporation of non-liquid crystalline mesogens into a polysiloxane side-chain LCE network lowered T_{NI}. More recently, McCracken et al. demonstrated that replacing the liquid crystal mesogen with a biphenyl mesogen with reduced π-π intermolecular interactions reduced the T_{NI}, even when the linkers and crosslinkers were unchanged.[18] Lastly, a number of studies have shown that LCEs synthesized in the nematic phase have a higher T_{NI} compared with those synthesized in the isotropic state. This was attributed to mesogen-mesogen interactions present in the nematic phase during crosslinking.[23,24] While these studies demonstrated that the T_{NI} is dependent on a number of network properties and synthesis conditions, we lack a comprehensive understanding of how T_{NI} varies in LCEs and how to predict changes in T_{NI} for specific changes in network structure and chemistry.

Here, we demonstrate LCEs with a tuneable actuation temperature by systematically varying the liquid crystal mass content. This was achieved by either incorporating a non-liquid crystalline

[a] Department of Materials Science and NanoEngineering, Rice University, Houston, Texas 77005, USA. E-mail: RafaelV@Rice.edu
[b] Department of Chemical and Biomolecular Engineering, Rice University, Houston, Texas 77005, USA.

† Electronic Supplementary Information (ESI) available: [details of any supplementary information available should be included here]. See DOI: 10.1039/cXsm00000x/

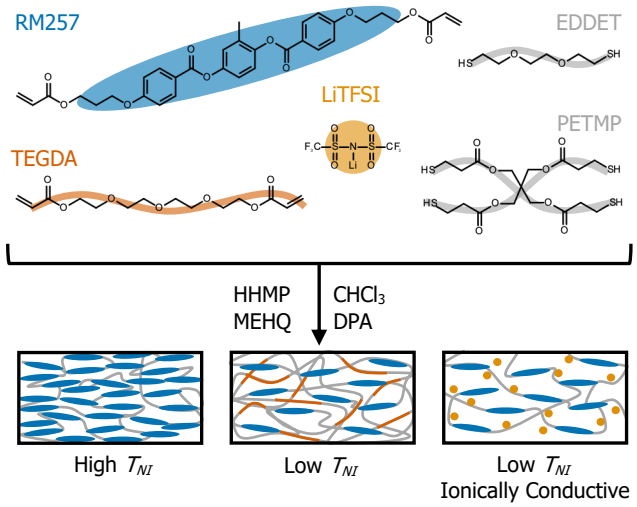

Fig. 1 Reaction scheme for the preparation of LCEs used in this study. LCEs with a high T_{NI} contain a higher content of liquid crystal mesogen RM257. LCEs with a low T_{NI} have lower RM257 content and are diluted by either non-mesogenic diacrylate TEGDA or lithium salt LiTFSI. EDDET and PETMP serve as chain-extenders and crosslinkers, respectively.

linker into the system or by incorporating a lithium salt (LiTFSI) into the network (Figure 1). The addition of lithium salt results in ionically conductive LCEs potentially useful as solid-state electrolytes, or sensors in stretchable electronics.[25–28]. For both of these systems, we found that the LCE T_{NI} varied linearly with the liquid crystal mass content which is consistent with previous liquid crystal theory and experiments.[22,29,30] Additionally, we present data on two other main-chain LCEs reported in the literature and show that the T_{NI} also varies linearly with liquid crystal mass content in these systems, regardless of liquid crystal mesogen, crosslink density, network genesis, or chemistry used. Therefore, while it is predictable that T_{NI} scales linearly with liquid crystal content it is surprising and useful that this one parameter accurately predicts the T_{NI} regardless of other parameters known to affect the thermo-mechanical properties of LCEs Further, we show that these data collapse onto a single master curve when the LCE T_{NI} is plotted relative to that of the pure mesogen, suggesting a general relationship between LCE T_{NI} and liquid crystal mass content which will be useful for quickly tuning the T_{NI} of new liquid crystalline mesogens. We also investigated the loss of maximum actuation strain in LCEs as the liquid crystal content is reduced and explored applications of LCEs with low T_{NI}. This work provides a method for tuning the actuation temperature of LCEs and provides insight into the relationship between T_{NI} and actuation strains in LCEs.

2 Experimental Methods

Materials and Methods

2,2'-(ethylenedioxy) diethanethiol (EDDET), pentaerythritol tetrakis (3-mercaptopropionate) (PETMP), 1,3-propanedithiol (PDT), tetra(ethylene glycol) diacrylate (TEGDA), 1,4-Bis-[4-(3-acryloyloxypropyloxy) benzoyloxy]-2- methylbenzene (RM257), chloroform, dipropyl amine (DPA), triethylamine (TEA), 4-methoxyphenol (MEHQ), and (2-hydroxyethoxy)-2-methylpropiophenone (HHMP) were obtained from commercial suppliers and used as received.

Preparation of Liquid Crystal Elastomers (LCEs)

LCEs were synthesized using previously reported methods.[31] LCEs were made with varying amounts of functional acrylate groups coming from TEGDA compared to RM257, thiol endgroups coming from PETMP, and overall excess acrylate functional endgroups compared to thiol. A table of the mass amount of reagents used to synthesize TEGDA LCEs can be found in Table S1. First, RM257, TEGDA, 0.5 wt % HHMP, and 0.25 wt % MEHQ were dissolved in chloroform (120 mg) at 70°C. MEHQ was added to prevent unintentional acrylate-acrylate polymerization before UV-curing. After the mixture cooled to room temperature EDDET and PETMP were added followed by a 2 wt % DPA solution in chloroform. The mixture was then vortexed to ensure proper mixing and placed under vacuum to remove any bubbles. Next, the mixture was deposited onto a glass slide cured at room temperature for at least 5 hours. After the first cure was complete, the LCE was heated to 80 °C under a vacuum of 30 mm hg for 5 hours to remove chloroform. Finally, the LCE was mechanically deformed to the desired shape and irradiated with 365 nm light for 10 minutes to complete the second cure step. Single-cure LCEs were made by a similar process but without HHMP or MEHQ added and an equimolar ratio of acrylate to thiol functional endgroups.

Lithiated LCEs were synthesized using a similar approach except various amounts lithium bis(trifluoromethanesulfonyl)imide (LiTSFI) (0 to 0.25 Li^+/EO mol) were added to the solution mixture prior to the first cure. Additionally, as lithium salts co-catalyze the thiol-acrylate Michael addition[32], we increased the volume of solvent by three times and used TEA instead of DPA. These changes prevented rapid polymerization. A table of the mass amount of reagents used to synthesize lithiated LCEs can be found in Table S2.

Liquid crystal mass content percentages were calculated as the total mass of liquid crystal mesogen divided by the total mass of network reagents, including liquid crystal mesogen, linker, crosslinker, and/or dopant (lithium salt)), multiplied by 100.

Construction of LCE fluidic Pump

LCE fluidic pumps were constructed by first making a flat LCE film with a thickness of ≈0.3mm. Films with three different regions each with a different T_{NI} were produced by making three different LCE mixtures with varying TEGDA content, as described in the preceding section. Equal amounts of each mixture were deposited onto a glass substrate and cured to produce one uniform LCE with three different T_{NI} regions. The film was then embossed using a 3/32-inch-thick basswood template, UV cured, and then adhered to a glass substrate using PDMS. This process is shown in Figure S1.

Dynamic Mechanical Analysis

Soft elastic plateaus were obtained using an ARES G2 (TA instruments) rheometer using a linear film tension clamp. Rectangular samples were loaded into the clamp and pulled at a linear strain rate of 200 %/min. The soft-elastic plateaus were identified as the region of the stress vs. strain curve where stress is near constant, i.e. a slope of near 0. This region was detected using python and SciPy's curve fit function to fit the experimental stress-strain data with three connected lines, the initial high slope elastic region, the near zero soft-elastic region, and the final higher slope stretching region. The lower and upper limits of the soft elastic region were estimated as the intersection of the fitted line for the soft elastic region with the initial and final higher slope regions, respectively.

Differential Scanning Calorimetry

The T_{NI}s of LCEs were obtained using a TA instruments Q20 DSC. Samples were heated and cooled at a ramp of 5^oC min^{-1}, and the T_{NI} was determined from the second heating cycle as the peak of the endothermic well.

Curvature, Flatness, and Actuation Strain

Curvature, flatness, fixity and actuation were determined using the same protocol reported previously.[31]. Briefly, curvature and flatness were determined by UV curing the LCE around a rod with known radius. The LCE was then imaged in the heated isotropic phase and again after it cooled to room temperature. Curvature was calculated by fitting a line to the curled edge of the LCE and normalizing the extracted radius of curvature of the LCE to the programmed one, i.e. the radius of the rod. An LCE that perfectly holds its programmed curvature has a normalized curvature, κ_n, of 1. Similarly, a flat line was fitted to the edge of LCE when heated and the flatness was calculated as the standard error for the flat line fitted to the LCE. An LCE that is perfectly flat in the isotropic phase has a flatness value f of 0. Actuation strain was determined by marking two dots on an LCE strip 10 mm apart prior to stretching the material. After stretching and UV curing, the strain was measured as the change of length between the two dots when the LCE was heated (contracted) above the T_{NI} divided by the distance between the dots when the sample was coooled (elongated) to room temperature.

Electrochemical impedance spectroscopy (EIS)

Li LCE films were cut into 1.5 cm^2 circles and then pressed into 2 stainless steal spacers. The spacers was placed in a 2032 size coin cell, and stainless steel contacts were welded to cell surface. The LCE film was placed in an oven for an hour before each temperature measurement was performed. The conductivity was measured using EIS (Autolab, Metrohm) over a frequency range of 1 MHz and 0.1 Hz at a voltage amplitude of 10 mV. The EIS measurement was fitted to an equivalent circuit to get a bulk electrolyte resistance, R, and the ionic conductivity σ was calculated from the formula $\sigma = d/RA$ where d is the sample thickness and A the cross-sectional area.

3 Results and discussion

We studied the impact that overall liquid crystal mass content has on the order-to-disorder transition temperature, T_{ODT} by preparing a series of LCEs with RM257 mesogen and diluted with either non-mesogenic linker TEGDA or lithium salt LiTFSI (see Fig. 1). We also collected data from other LCEs in the literature, specifically LCEs containing RM257, MR82, or BP4OH mesogens. These LCEs were chosen as there is extensive data available on the T_{ODT}s of each material. RM257 and RM82 are structurally similar di-acrylate mesogens. They can be incorporated into LCEs using the aza-Michael addition or thiol-acrylate Michael additions to produce nematic LCEs that can be aligned using surface anchoring, 3D printing, and mechanical defrmation.[12,13,15,21,31,33]. BP4OH is a biphenyl epoxy mesogen with a smectic phase and a much higher T_{ODT} ((160^{o}C) than RM257 (70^{o}C) or RM82 (85^{o}C)[17]. It has been used to produce dynamic, reconfigurable LCEs that are aligned by mechanical deformation.[16,34,35]

We used dynamic scanning calorimetry (DSC) to measure the T_{NI}s for a series of RM257 LCEs varying in liquid crystal mass content and plotted these values along with data for other RM257 LCEs reported in the literature (see Fig. 2a). For the TEGDA LCE series, we incorporated a non-liquid crystalline diacrylate, TEGDA, while maintaing the same overall acrylate to thiol molar ratio in the network. This results in a series of RM257 LCEs with the same network crosslink density but varying in liquid crystal mesogen content. Similarly, for the lithiated LCEs (Li LCEs), varying amounts of lithium salt was added while keeping the same molar ratio of network-forming reagents. This produced a series of Li LCEs with similar network properties but varying in liquid crystal mass content. As expected, the order-to-disorder transition temperature T_{ODT} varied strongly with the overall liquid crystal mesogen content of the networks. The relationship between T_{ODT} and liquid crystal mass content was linear over a wide range (from approximately 65 to 85 wt % liquid crystal and T_{ODT}s ranging from 25 to 150°C) for both LCE network series prepared (see Fig. 2a). This relationship is consistent with the Maier-Saupe theory of liquid crystals, which predicts a linear dependence of the order-disorder transition on liquid crystal density[37,38].

We also included data from published reports on RM257 LCEs, and these data also show a linear relationship between T_{NI} and liquid crystal mass content. While a variety of factors influence T_{NI}, the plot suggests that liquid crystal mass content is the most important factor that influences T_{NI}. For example, prior studies by Saed *et al.*[20] demonstrated that the crosslink density affected T_{NI} even when the liquid crystal mass content was held constant. This is reflected in Fig. 2a in the points near 75% liquid crystal mass content. However, the variation in T_{NI} for these samples is small compared to the much stronger variation observed with liquid crystal mass content. Similarly, other studies reported that stiffer linkers or network genesis influence T_{NI}.[21]? These effects are reflected in Fig. 2a, but the plot demonstrates that T_{NI} is much more strongly dependent on the overall liquid crystal mass content.

Next, we compiled published data to compare the T_{ODT}s of RM82, RM257, and BP4OH LCEs as a function of liquid crystal

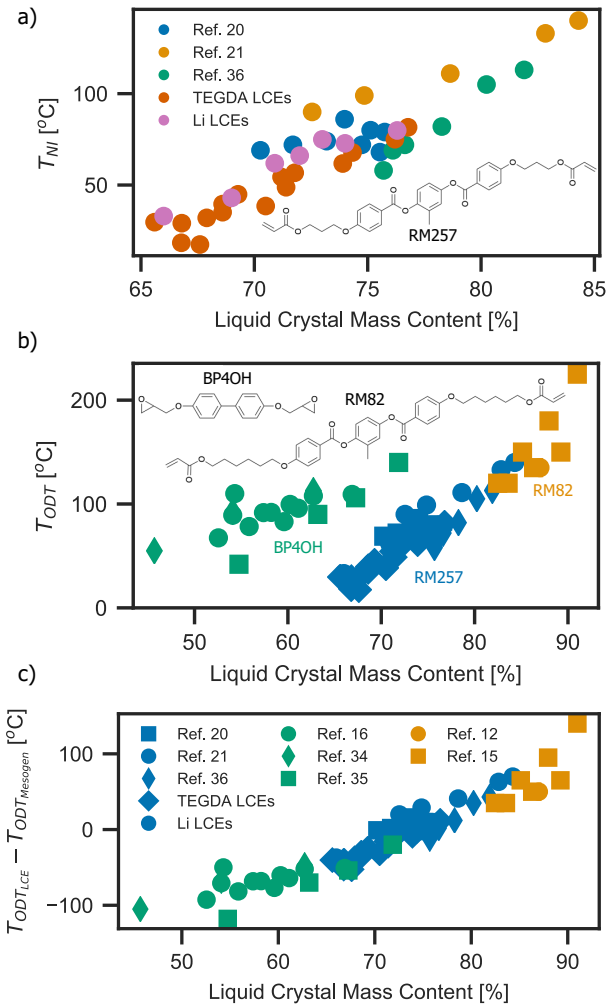

Fig. 2 Order-to-disorder transition temperature as a function of liquid crystal mass content for LCEs with a) RM257 or b and c) RM257, RM82, or BP40H mesogens. a) T_{NI} of RM257 LCEs as a function of overall liquid crystal (RM257) mass content. b) Liquid crystal to isotropic transition temperature, T_{ODT}, as a function of liquid crystal mass content for RM257, RM82, and BP4OH LCEs. c) T_{ODT} for LCEs relative to that for pure mesogen for RM257, RM82, and BP4OH LCEs. The values for RM257 LCEs were acquired as described herein for TEGDA and LiLCE samples. Additional data for RM257 LCEs is reported in references Saed *et al.*[20,21], Merkel *et al.*[36]. Data for RM82 and BP4OH LCEs is reported in references Ware *et al.*[12], Ahn *et al.*[15], and Zhu *et al.*[16], Li *et al.*[34], Gablier *et al.*[35]. Symbol references for b) consistent with c).

mass content (Figure 2b). Each type of LCE exhibits a linear relationship between liquid crystal mass content and T_{ODT}. Additionally, the trends for RM82 and RM257 overlap, which might be expected as RM82 and RM257 are very similar mesogens. The RM82 LCEs were synthesized via the aza-Michael addition reaction rather than the thiol-Michael addition reaction used to produce RM257 LCEs, resulting in a higher liquid crystal mass content for the RM82 LCEs. Additionally, RM82 were aligned by confinement between surfaces while the RM257 LCEs were synthesized in either the nematic or isotropic state using bulk mechanical or shear-extrusion 3D printing alignment, but both series fall on the same trendline for T_{ODT} vs. liquid crystal mass content.

The T_{ODT} values are significantly higher for BP4OH compared with RM257 or RM82 LCEs at the same liquid crsytal mass content. However, these T_{ODT}s can be plotted relative to that for the pure mesogen (Figure 2c). When plotted in this way, the T_{ODT} for all LCEs falls on a master linear curve. This is remarkable given the variations in liquid crystal mesogen, preparation method, alignment method, and network chemistry across these samples, which include data from eight different reports in addition to the samples prepared in this study. This relationship implies that liquid crystal mesogen content is the most important factor governing the T_{ODT} of these LCEs and that a reliable approximation of the T_{ODT} can be obtained by knowing the T_{ODT} of the pure mesogen and the liquid crystal content of the LCE. Interestingly, above 75% liquid crystal mass content, the LCEs exhibit higher T_{ODT}s than of the pure mesogen. These LCEs contain very short linkers, which may reduce the flexibility of the liquid crystal mesogens and result in an increase in the T_{ODT}.

Next, we studied the relationship between the liquid crystal mass content and thermoreversible shape changes in LCEs. First, we investigated the width of the soft elastic plateau in polydomain LCEs. Polydomain LCEs exhibit 'soft elasticity', in which the LCE can be deformed with little or no increase in stress. This phenomenon is related to the rotation of the liquid crystal orientation and the anisotropic polymer chain conformation during mechanical deformation.[30,39,40]. Stretching a polydomain LCE results in three distinct stress-strain regions: 1) an initial region where stress increases with strain due to deformation of the network, 2) a region where stress does not increase with strain or increases very weakly, and 3) a region where stress again increases with strain. These distinct regions for RM257 LCEs are shown in Fig. 3a, where the soft elastic region is highlighted. We observed that the width of the soft elastic plateu decreased as the TEGDA content increased. For LCEs with no TEGDA, the length of the soft-elastic plateau was around 100%, and the soft elastic region decreased to approximately 20 % for 20 wt% TEGDA. This reflects both a decreased polymer chain anisotropy and weaker coupling between the liquid crystal orientation and network deformation and is consistent with prior knowledge soft-elasticity is directly coupled to the nematic order parameter[30]. Decreased chain anisotropy and weaker coupling are expected as the liquid crystal content decreases. For the LCE with 20% TEGDA, the soft elastic plateau is nearly absent. We observed a region of strains where the stress-strain slope was only slightly lower than that at low and high strains, and this is highlighted in Fig. 3a.

We next determined the maximum reversible actuation achievable for each LCE by applying a uniaxial strain to deform each sample to 125% of the initial length followed by UV curing in the deformed state. The resulting sample was then heated and cooled to measure the actuation strain. The maximum actuation strains decreased with increasing amount of TEGDA (Fig. 3b and c) . This again reflects a decrease in the strength of coupling between liquid crystal ordering and network deformation as the liquid crystal content decreases and is consistent with prior studies focused on decreasing the actuation temperature.[22]. Importantly, we observed that the maximum actuation measured closely matched the length of the soft elastic plateau measured for polydomain LCEs (Fig. 3b). This suggests that measuring the soft

elastic plateau for polydomain LCEs is a convenient method to quantify the maximum actuation achieveable through alignment and crosslinking while simultaneously obtaining other mechanical properties of the material such as elastic modulus, strain to failure, or toughness.

The reduction in maximum actuation strain with decreasing liquid crystal content has practical implications for applications that require low T_{NI}s since diluting the liquid crystal content reduces the maximum actuation strains achievable. If a large actuation response at low actuation temperatures is desired, low T_{NI} mesogens are required to produce low T_{NI} LCEs with high liquid crystal mass contents[18] or devices should be engineered to produce bending deformations, which can produce significant curvature with even small strains. To demonstrate actuation at near-ambient temperatures, we developed a prototype LCE 'Band-Aid' that has a T_{NI} of $\approx 40^o$C and wraps around the finger when touched (Fig. 3d). This was achieved by making a bilayer of an LCE and kapton tape. The maximum linear strain achievable by the LCE was only about 50%, but this is sufficient to achieve significant bending curvatures.[41] Therefore, the low T_{NI} 'band-aid' LCE shown here can produce significant actuation responses with very modest temperature changes. This is the first LCE demonstrated to actuate in response to body heat and could be useful for future designs of biomedical devices.

Next, we optimized the LCE network crosslink density for samples with low T_{NI} to enable more complex shape changes. In a previous paper, we showed that optimizing the relative crosslink densities during the first and second network crosslinking reactions was important for mechanically programming shape changes in LCEs. Optimized LCE compositions were capable of large and reversible shape actuations, even between two non-planar shapes. However, we have not explored this for LCEs with varying liquid crystal mesogen contents. To optimize the network properties, we started with a previously optimized network composition of 10% excess acrylate and 25% thiols attributed to PETMP. We fabricated LCEs in two steps, as an initially flat strip after the first crosslinking reaction and curled around a rod after the second crosslinking reaction. A properly optimized LCE is curled at low temperatures and is perfectly flat at temperatures above the T_{NI}. To quantify this shape-reversibility, we measured the normalized curvature κ_n, which is the room temperature radius of curvature divided by the programmed radius of curvature, and flatness parameter f, which is the standard error of a line fitted to the edge-on profile of the heated LCE. The values for κ_n and f should be 1 and 0, respectively, for an ideal, shape-reversible LCE.[31] While all fabricated TEGDA LCEs were capable of holding programmed low-strain curvatures, they were unable to produce a flat sheet at elevated temperatures, as demonstrated by $f > 0$ for the 10 and 15% TEGDA contents (Fig. 4a).

Therefore, optimization of the RM257 network crosslink densities was required to achieve both large and reversible shape actuation along with a low T_{NI}. This was expected as when a new monomer, TEGDA, is added to the system the degree of crosslinking during each curing step changes. As TEGDA is added to the LCE, there is a greater excess of acrylate that reacts during the second curing step, producing a sample which is able to hold the shape during the second curing reaction but is unable to return to the initially flat sample shape. We started by optimizing the network structure for the 10% TEGDA LCE (Fig. S2) by varying the amount of PETMP and excess acrylate in the system. We then found the optimized composition for the 10% TEGDA LCE where κ_n and f were near 1 and 0, respectively. The ideal composition for this LCE has 10% excess acrylate and 40% of thiol attributed to PETMP.

Next, instead of repeating this optimization process for the other TEGDA contents, we performed an extrapolation to approximate the optimized network composition for the RM257 with 5 or 10 wt % TEGDA. These values are shown in Fig. 4b. We then measured κ_n and f for each LCE as shown in Fig. 4b. These samples were much closer to the ideal values of κ_n and f are near 1 and 0, respectively, compared with the original LCE formulations (Fig. 4b), indicating an optimized or near-optimal network composition.

To demonstrate a potential use of mechanically programmed LCEs with varying T_{NI}s, we developed a prototype fluidic pump that directionally pumps liquid when uniformly heated as shown in Fig. 4. Flat films were prepared that comprised of three different compositions of LCE with T_{NI}s of 57, 67, and 77 ^{o}C. The resulting LCE film contained three distinct T_{NI} regions (Fig. 4c). The film was then embossed and UV cured to program a raised fluidic channel and adhered to a glass substrate. When uniformly heated, the lowest T_{NI} section collapses first to pump any liquid in the channel towards the higher T_{NI} sections. Photographs of the prototype LCE pump sequentially collapsing to expel water when heated under an IR heat lamp are shown in Fig. 4. This method seamlessly creates LCE films with distinct and tunable T_{NI} regions that can be mechanically programmed into arbitrary shapes is potentially useful for many applications where sequential actuation is required.

Next, we explored the use of the lithium salt LiTSFI as an additive to lower the T_{NI} and produce ionically conductive LCEs.[27] Lithiated ethylene oxide polymers can form crystalline domains at room temperature, resulting in materials with poor ionic conductivity. However, the ionic conductivity improves dramatically when the lithiated polymers are heated above the melting temperature of the crystallized EO segments (approximately 30-35^{o}C) This demonstrates a strong coupling of material phase to the conductivity. LCEs have an additional phase transition at the T_{NI} which could further serve to modulate the ionic conductivity. We therefore were interested in investigating ionic conduction in lithiated LCEs and understanding the impact of nematic or isotropic ordering on ionic conductivity. We added LiTFSI with molar ratios ranging from 0 to 0.125 of Li^+/EO, as previous studies have shown maximum ionic conductivity for liquid crystal/EO oligomers at a loading ratio of 0.1 Li^+/EO.[42] Comparing the actuation strains and T_{NI}s of the lithiated LCEs with TEGDA LCEs, we observed very similar trends of linear decrease of actuation temperatures and strains as a function of liquid crystal mass content as shown in Fig. 5. This further supports our claim that T_{NI} is largely independent of chemistry or crosslink density of the LCE and governed primarily by the liquid crystal mass content in the network and the T_N of the mesogen used to produce the LCE.

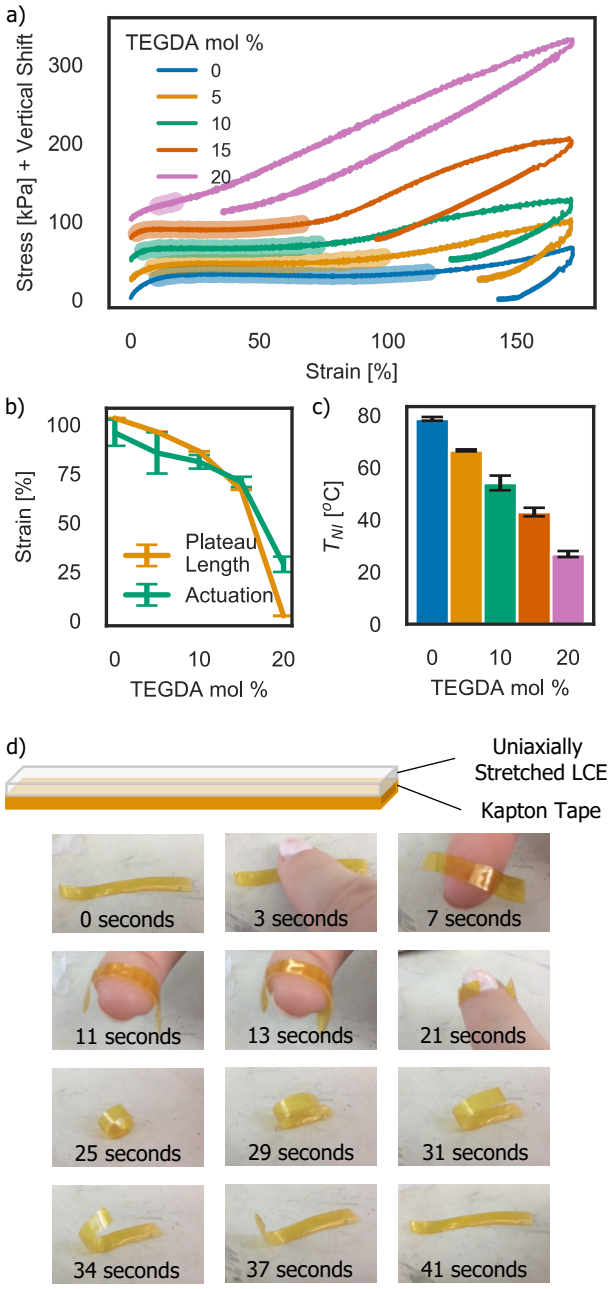

Fig. 3 Characterization of TEGDA LCEs with varying amounts of non-mesogenic TEGDA monomer and demonstration of an LCE band-aid that responds to body temperature. a) Stress-strain behavior for uniaxial extension of TEGDA LCEs with varying amounts of TEGDA. The highlighted region indicates the soft elastic plateau, over which the samples deform with little or no increase in stress. As the TEGDA content increases, the breadth of the soft-elastic plateau decreases. The stress-strain curves were vertically shifted by 25, 50, 75, and 100 kPa for 5, 10, 15, and 20 TEGDA mol %, respectively. b) Comparison of the extent of the soft-elastic plateau (orange) and maximum programmable actuation strains (green) of LCEs for varying amounts of TEGDA. As the TEGDA content increases, the maximum programmable strain and length of the soft elastic plateau decrease. (n = 3 for plateau length, n = 5 for actuation) c) T_{NI} as a function of TEGDA content in the LCE. (n = 3) d) Schematic and images of a low T_{NI} (TEGDA amount = 15%) LCE bilayer that curls around a finger in response to body heat. The LCE returns to its initial shape upon removing from the body and returning to ambient temperatures.

In addition to the typical DSC nematic-to-isotropic peak around 70^{o}C that decreases with increasing lithium loading, we observed a second peak around 30^{o}C as shown in Fig. S3. This second peak is consistent with the crystallization/melting of lithiated EO.[28] A phase diagram constructed from DSC data is shown in Fig. 5. As previously demonstrated, the T_{NI} decreases linearly as lithium is added to the system. For low lithium loadings (< 0.17 Li^+/EO) there is a distinct temperature range where the EO regions are no longer crystalline but the LCE exhibits a nematic liquid crys-

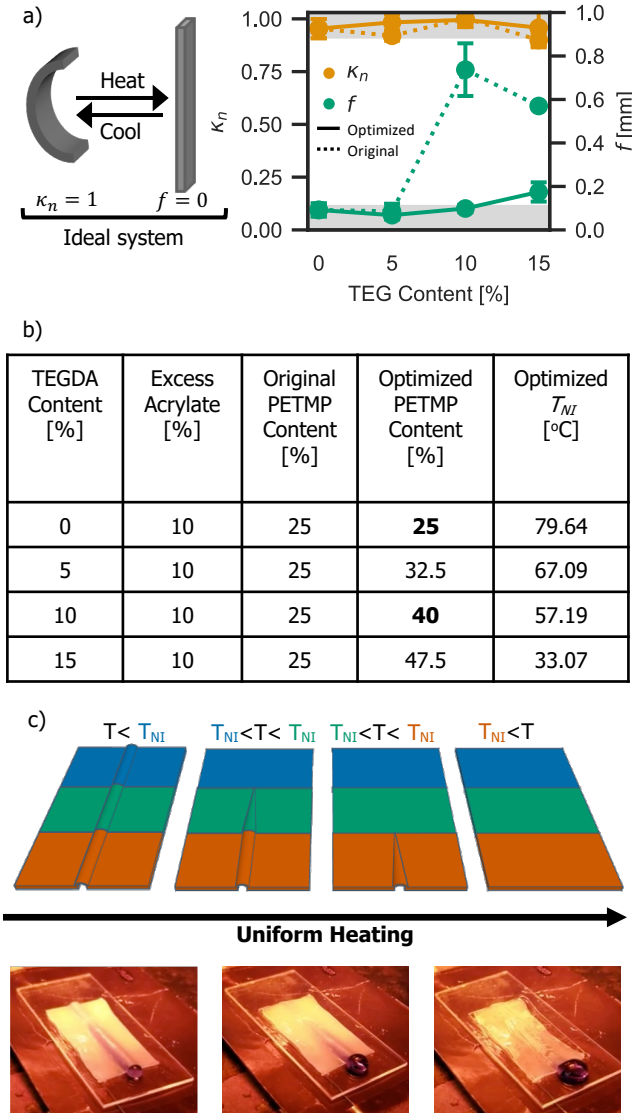

b)

TEGDA Content [%]	Excess Acrylate [%]	Original PETMP Content [%]	Optimized PETMP Content [%]	Optimized T_{NI} [°C]
0	10	25	**25**	79.64
5	10	25	32.5	67.09
10	10	25	**40**	57.19
15	10	25	47.5	33.07

Fig. 4 a) Diagram of ideal mechanically shape-programmable LCE that holds its programmed curvature (κ_n) at $T < T_{NI}$ and returns a flat sheet ($f = 0$) at $T > T_{NI}$ and plot of (κ_n) and ($f = 0$) for the original and optimized compositions of TEGDA LCEs. (n = 5) b)Optimized compositions of LCEs with varying TEGDA % content. Bold values were experimentally obtained and the non-bold values were extrapolated from the bold values. c)**TOP** Schematic of LCE synthesized using three different compositions to obtain an LCE fluidic channel that sequentially collapses upon uniform heating to produce directional fluidic pumping. T_{NI}s of LCE regions are 57, 67, and 77 ^{o}C. **BOTTOM** Photograph of the fluidic pump actuated with an IR heat lamp.

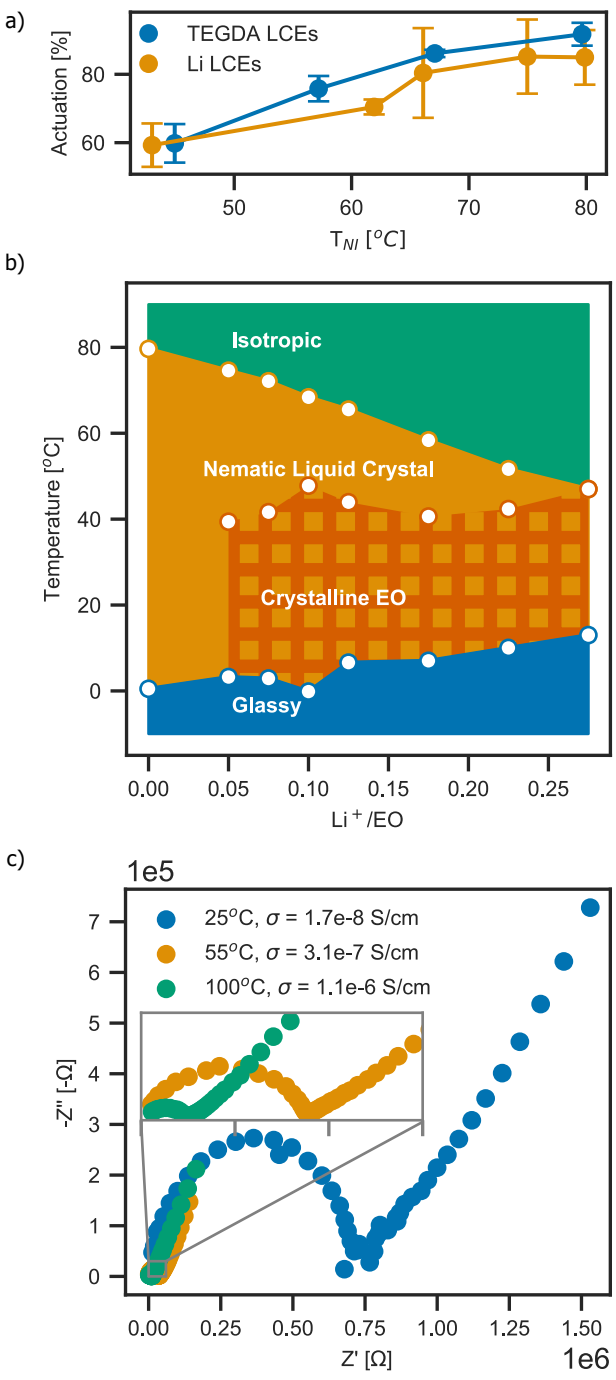

Fig. 5 a) Actuation strains of lithiated LCEs compared with TEGDA LCEs. (n = 5) b) Phase diagram of lithiated LCEs. c) Nyquist plots of a 0.1 Li$^+$/EO lithiated LCE at room temperature, 55^{o}C, and 100^{o}C.

tal phase. However, as more lithium is added and the T_{NI} decreases further, the EO crystallization and nematic-to-isotropic peaks merge indicating that the LCE transitions directly from the crystalline EO/nematic liquid crystal phase to the isotropic phase.

Nyquist plots of a 0.1 Li$^+$/EO polydomain LCE collected at room temperature, 55^{o}C, and 100^{o}C are shown in Fig. 5. Most lithiated EO polymers exhibit two large increases in ionic conductivity between room temperature and temperatures higher than the EO crystal melting temperature.[43] However, this data shows an order of magnitude increase in conductivity between room temperature when the LCE EO regions are crystallized, at 55 ^{o}C when EO regions are not crystalline but the LCE is in the nematic phase, and at 100^{o}C when the LCE is in the isotropic phase, showing that nematic ordering has a detrimental impact on ionic conduction. Tuning the T_{NI} relative to the EO crystal melting temperature therefore provides a simple approach to tune ionic conductivity. Future work will focus on further studying the ionic conductivity of LCEs at various lithium loadings and fully mapping the conductivity to the phase behavior of LCEs.

4 Conclusion

We show that the T_{NI} of LCEs varies linearly with the mass % of liquid crystals in the polymer network and is much less dependent on liquid crystal mesogen, cross-link density, linker composition, network genesis, or chemistry. We can readily predict and tune the T_{NI} of LCEs by incorporating either TEGDA linkers or lithium salts to reduce the density of liquid crystals in the elastomer. However, the maximum actuation strain and soft-elasticity of LCEs also decreases with non-liquid-crystalline fillers, which might be undesirable for some applications. We show that crosslink-density optimization of TEGDA LCEs with low T_{NI}s results in mechanically programmable LCEs and demonstrate potential appliaction of these low T_{NI} LCEs by developing a prototype self-wrapping LCE 'band-aid' that reacts to body heat and an LCE fluidic channel that directionally pumps liquid when uniformly heated. Additionally, we show that lithium salts incorporated into an LCE containing ethyl oxide groups reduces the T_{NI} and results in a phase-dependent ionically conductive polymer with potential applications as sensors.

Conflicts of Interest

The authors declare no competing financial interests.

Acknowledgements

The authors acknowledge support from the the Army Research Office Chemical Sciences Division (W911NF1810289), and the Shared Equipment Authority at Rice University.

References

1 K. M. Herbert, H. E. Fowler, J. M. McCracken, K. R. Schlafmann, J. A. Koch and T. J. White, *Nat. Rev. Mater.*, 2022, **7**, 23–38.

2 A. Agrawal, O. Adetiba, H. Kim, H. Chen, J. G. Jacot and R. Verduzco, *J. Mater. Res.*, 2015, **30**, 453–462.

3 H. Zeng, O. M. Wani, P. Wasylczyk, R. Kaczmarek and A. Priimagi, *Adv. Mater.*, 2017, **29**, 1–7.

4 Q. Liu, T. Jain, C. Peng, F. Peng, A. Narayanan and A. Joy, *Macromolecules*, 2020, **53**, 3690–3699.

5 D. Mistry, M. Nikkhou, T. Raistrick, M. Hussain, E. I. Jull, D. L. Baker and H. F. Gleeson, *Macromolecules*, 2020, **53**, 3709–3718.

6 A. Kotikian, J. M. Morales, A. Lu, J. Mueller, Z. S. Davidson, J. W. Boley and J. A. Lewis, *Adv. Mater.*, 2021, **33**, 1–9.

7 H. Tian, Z. Wang, Y. Chen, J. Shao, T. Gao and S. Cai, *ACS Appl. Mater. Interfaces*, 2018, **10**, 8307–8316.

8 Z. Li, Y. Yang, Z. Wang, X. Zhang, Q. Chen, X. Qian, N. Liu, Y. Wei and Y. Ji, *J. Mater. Chem. A*, 2017, **5**, 6740–6746.

9 C. Yuan, S. Ai, J. Wu, T. Wang, H. J. Qi, Y. Mao, M. Isakov, Z. Ding and M. L. Dunn, *Sci. Rep.*, 2016, **6**, 1–13.

10 C. Wang, K. Sim, J. Chen, H. Kim, Z. Rao, Y. Li, W. Chen, J. Song, R. Verduzco and C. Yu, *Adv. Mater.*, 2018, **30**, 43–71.

11 A. Agrawal, H. Chen, H. Kim, B. Zhu, O. Adetiba, A. Miranda, A. Cristian Chipara, P. M. Ajayan, J. G. Jacot and R. Verduzco, *ACS Macro Lett.*, 2016, **5**, 1386–1390.

12 T. H. Ware, M. E. McConney, J. J. Wie, V. P. Tondiglia and T. J. White, *Science (80-.).*, 2015, **347**, 982–984.

13 C. P. Ambulo, J. J. Burroughs, J. M. Boothby, H. Kim, M. R. Shankar and T. H. Ware, *ACS Appl. Mater. Interfaces*, 2017, **9**, 37332–37339.

14 A. Kotikian, R. L. Truby, J. W. Boley, T. J. White and J. A. Lewis, *Adv. Mater.*, 2018, **30**, 1–6.

15 S. K. Ahn, T. H. Ware, K. M. Lee, V. P. Tondiglia and T. J. White, *Adv. Funct. Mater.*, 2016, **26**, 5819–5826.

16 B. Zhu, M. G. Barnes, H. Kim, M. Yuan, H. Ardebili and R. Verduzco, *Sensors Actuators, B Chem.*, 2017, **244**, 433–440.

17 M. Giamberini, E. Amendola and C. Carfagna, *Mol. Cryst. Liq. Cryst. Sci. Technol. Sect. A. Mol. Cryst. Liq. Cryst.*, 1995, **266**, 9–22.

18 J. M. McCracken, B. R. Donovan, K. M. Lynch and T. J. White, *Adv. Funct. Mater.*, 2021, **31**, 1–10.

19 H. H. Yoon, D. Y. Kim, K. U. Jeong and S. K. Ahn, *Macromolecules*, 2018, **51**, 1141–1149.

20 M. O. Saed, A. H. Torbati, C. A. Starr, R. Visvanathan, N. A. Clark and C. M. Yakacki, *J. Polym. Sci. Part B Polym. Phys.*, 2016, **55**, 157–168.

21 M. O. Saed, R. H. Volpe, N. A. Traugutt, R. Visvanathan, N. A. Clark and C. M. Yakacki, *Soft Matter*, 2017, **13**, 7537–7547.

22 M. O. Saed, C. P. Ambulo, H. Kim, R. De, V. Raval, K. Searles, D. A. Siddiqui, J. M. O. Cue, M. C. Stefan, M. R. Shankar and T. H. Ware, *Adv. Funct. Mater.*, 2018, **29**, 1–9.

23 T. S. Hebner, C. N. Bowman and T. J. White, *Macromolecules*, 2021, **54**, 4023–4029.

24 J. S. Biggins, M. Warner and K. Bhattacharya, *J. Mech. Phys. Solids*, 2012, **60**, 573–590.

25 L. Shi, T. Zhu, G. Gao, X. Zhang, W. Wei, W. Liu and S. Ding, *Nat. Commun.*, 2018, **9**, 1–7.

26 T. Kato, M. Yoshio, T. Ichikawa, B. Soberats, H. Ohno and M. Funahashi, *Nat. Rev. Mater.*, 2017, **2**, 1–20.

27 Z. Xue, D. He and X. Xie, *J. Mater. Chem. A*, 2015, **3**, 19218–19253.

28 B. Kim, H. Kang, K. Kim, R. Y. Wang and M. J. Park, *ChemSusChem*, 2020, **13**, 2271–2279.

29 B. Donnio, H. Wermter and H. Finkelmann, *Macromolecules*, 2000, **33**, 7724–7729.

30 M. Warner and E. M. Terentjev, *Liquid Crystal Elastomers*, Oxford University Press, Oxford, England, 2003.

31 M. Barnes and R. Verduzco, *Soft Matter*, 2019, **15**, 870–879.

32 K. Jiang, J. Wang, C. Zuo, S. Li, S. Li, D. He, H. Peng, X. Xie, R. Poli and Z. Xue, *Macromolecules*, 2020, **53**, 7450–7459.

33 D. R. Merkel, R. K. Shaha, C. M. Yakacki and C. P. Frick, *Polymer (Guildf).*, 2019, **166**, 148–154.

34 Y. Li, C. Pruitt, O. Rios, L. Wei, M. Rock, J. K. Keum, A. G. Mcdonald and M. R. Kessler, *Macromolecules*, 2015, **48**, 2864–2874.

35 A. Gablier, M. O. Saed and E. M. Terentjev, *Macromolecules*, 2020, **53**, 8642–8649.

36 D. R. Merkel, N. A. Traugutt, R. Visvanathan, C. M. Yakacki and C. P. Frick, *Soft Matter*, 2018, **14**, 6024–6036.

37 G. R. Luckhurst and C. Zannoni, *Nature*, 1977, **267**, 412–414.

38 M. A. Cotter, *J. Chem. Phys.*, 1977, **66**, 1098–1106.

39 D. Agra-Kooijman, W. Ren, P. McMullan, S. Kumar, A. Griffin and S. Dey, *Crystals*, 2013, **3**, 363–390.

40 N. A. Traugutt, R. H. Volpe, M. S. Bollinger, M. O. Saed, A. H. Torbati, K. Yu, N. Dadivanyan and C. M. Yakacki, *Soft Matter*, 2017, 7013–7025.

41 S. Timoshenko, *J. Opt. Soc. Am.*, 1925, **11**, 233.

42 T. Ohtake, K. Ito, N. Nishina, H. Kihara, H. Ohno and T. Kato, *Polym. J.*, 1999, **31**, 1155–1158.

43 M. Ghelichi, N. T. Qazvini, S. H. Jafari, H. A. Khonakdar, Y. Farajollahi and C. Scheffler, *J. Appl. Polym. Sci.*, 2013, **129**, 1868–1874.